



HAL
open science

Molecular Mechanism Underpinning Stable Mechanical Performance and Enhanced Conductivity of Air-Aged Ionic Conductive Elastomers

Burebi Yiming, Zhaoxin Zhang, Yuchen Lu, Xingang Liu, Costantino Creton, Shuze Zhu, Zheng Jia, Shaoxing Qu

► **To cite this version:**

Burebi Yiming, Zhaoxin Zhang, Yuchen Lu, Xingang Liu, Costantino Creton, et al.. Molecular Mechanism Underpinning Stable Mechanical Performance and Enhanced Conductivity of Air-Aged Ionic Conductive Elastomers. *Macromolecules*, 2022, 55 (11), pp.4665-4674. 10.1021/acs.macromol.2c00161 . hal-03951100

HAL Id: hal-03951100

<https://hal.science/hal-03951100>

Submitted on 23 Jan 2023

HAL is a multi-disciplinary open access archive for the deposit and dissemination of scientific research documents, whether they are published or not. The documents may come from teaching and research institutions in France or abroad, or from public or private research centers.

L'archive ouverte pluridisciplinaire **HAL**, est destinée au dépôt et à la diffusion de documents scientifiques de niveau recherche, publiés ou non, émanant des établissements d'enseignement et de recherche français ou étrangers, des laboratoires publics ou privés.

Molecular Mechanism Underpinning Stable Mechanical Performance and Enhanced Conductivity of Air-Aged Ionic Conductive Elastomers

Burebi Yiming,^{1,2,§} Zhaoxin Zhang,^{1,§} Yuchen Lu,¹ Xingang Liu,³ Costantino Creton,^{2,*} Shuze Zhu,^{1,*} Zheng Jia,^{1,*} Shaoxing Qu¹

¹Key Laboratory of Soft Machines and Smart Devices of Zhejiang Province, Center for X-Mechanics, Department of Engineering Mechanics, Zhejiang University, Hangzhou, 310027, China;

²Sciences et Ingénierie de la Matière Molle, ESPCI Paris, Université PSL, CNRS, Sorbonne Université, 75005 Paris, France

³State Key Laboratory of Polymer Materials Engineering, Polymer Research Institute of Sichuan University, Chengdu, 610065, China.

*E-mail: (C. Creton) costantino.creton@espci.psl.eu; (Z. Jia) zheng.jia@zju.edu.cn; (S.Z. Zhu) shuzezhu@zju.edu.cn

ABSTRACT

Ionic conductive elastomers (ICEs), thanks to their liquid-free nature, have emerged as one of the most promising candidates for conductors in soft ionotronics. Notably, most ionotronic devices need to work in ambient environments where the presence of water molecules is ubiquitous. Thus far, the long-term impact of ambient water on the performances of ICEs remains virtually unexplored. Here we show that air-aged ICEs absorb a very low amount of environmental water (~0.3-0.6 wt% of the ICEs), which endows ICEs with stable mechanical performance and strongly boosted conductivity. We study the underlying molecular mechanism and clarify that the scission of lithium bonds between lithium ions and elastomer chains provoked by diffusing water molecules accounts for the observed changes in ICE properties. This work provides guidance for the practical mass application of ICE-based soft ionotronics in ambient environments.

■ INTRODUCTION

The interdisciplinary field of soft ionotronics is advancing rapidly despite its recent origin¹. Significant achievements have been demonstrated with applications as diverse as biomimetics²⁻⁵, energy harvesting⁶⁻⁸, multimodal sensing⁹⁻¹², and other functional devices^{5,13-17}. As a key component of soft ionotronics, intrinsically stretchable ionic conductors are required for the development of high-performance soft ionotronic devices. The prevailing stretchable ionic conductors can be categorized into two types, namely, liquid-based (e.g., electrolyte water, ionic liquid) ionic conductors and liquid-free ionic conductors.

Hydrogels containing dissolved salts emerge as the prototypical example of liquid-based ionic conductors. Salt-containing hydrogels have demonstrated their advantages of high ionic conductivity, optical transparency, stretchability, and prominent biocompatibility, for a wide variety of applications such as skin-like ionotronic devices¹⁸⁻²⁰, artificial axons², triboelectric nanogenerators⁶, and electroluminescent devices²¹⁻²³. These devices, however, suffer from key shortcomings inherent to water-based electrolytes, which may easily evaporate or leak. According to the present consensus, the introduction of salts or chemicals into hydrogels can only slow down but hardly prevent the evaporation of water, which are impediments to the stable operation of hydrogel-based ionotronic devices over long periods of time^{1,24-26}. In addition, ionotronic devices based on hydrogels are often plagued by weak adhesion of hydrogels to other functional materials, such as elastomers, metals, and ionogels, due to the fluid nature of water --

the majority constituent of hydrogels -- which changes neighbor readily and cannot transfer stresses. The last few years have witnessed transformative advances in achieving tough bonding of hydrogel to other materials, but the adhesion method still involves complicated and material-specific treatment processes²⁷⁻³¹.

Another representative family of liquid-based ionic conductors is ionogels, which are polymeric gels swollen by ionic liquids (ILs). Most of the ILs are stable and nonvolatile, thereby endowing ionogels with high ionic conductivity, broader working temperature than hydrogels, wide electrochemical window, as well as good mechanical ruggedness³²⁻³⁴. In this respect, various soft ionotronic devices that can work in harsh conditions have been demonstrated with ionogels. Examples include ionotronic sensors that can monitor mechanical motions in extreme environments (e.g., high vacuum and high humidity)³⁵, triboelectric nanogenerators that can operate at both high and low temperatures⁷, and ionic cables that can function under water²¹. However, one major problem faced by the ionogel system is the degradation of ionic conductivity under mechanical loads (such as squeezing) or after long-term exposure to open air, largely due to the leakage of IL^{12,36,37}. Moreover, the electrical and mechanical properties of ionogels often conflict — introduction of IL, the key conducting constituent of ionogels, leads to enhanced ionic conductivity but diminished strength and modulus^{5,12,38-40} — so that ionogels based on IL struggle to attain both properties.

In light of these challenges common to liquid-based ionic conductors, enormous efforts have

been devoted to the development of liquid-free ionic conductors for soft ionotronics, by avoiding the incorporation of liquid components. Liquid-free ionoelastomers, in which either cations or anions are fixed to the elastomer network and the other ionic species are mobile, and ionic conductive elastomers (ICEs), which in contrast consist of elastomer networks and mobile cations and anions, have been reported in the last few years⁴⁰⁻⁴⁶. These materials are liquid-free and thus do not suffer from limitations inherent to the liquid constituents. Very recently, we developed a new type of ICE, in which the elastomer networks host lithium cations and associated anions via lithium bonds and hydrogen bonds, respectively. The material outperforms other state-of-the-art ICEs in terms of mechanical properties, exhibiting high strength, fracture toughness, stretchability, self-healing ability, strong adhesion to many materials, and desirable 3D printability as well³⁸. The discovery of mechanically robust ICEs paves the way for developing soft ionotronic devices with improved stability and durability relative to their liquid-based counterparts.

However, it is important to recognize that ionotronic devices inevitably work under ambient conditions in which the presence of water molecules is ubiquitous. ICEs rely predominantly on ions as charge carriers, and a wide variety of ions such as lithium cations (Li^+) are hygroscopic, capable of attracting water molecules from ambient environments and holding them among their polymer networks. For this reason, uncovering the effect of ambient water on the ICEs is essential for enabling ambient mass application of ICE-based ionotronic devices, and thus is of

significant practical interest in the field of soft ionotronics. Yet while these new stretchable ionic conductors emerged around 2018 and have been thriving since 2020^{38,40-46}, the influence of ambient water on ICEs in terms of their mechanical and electrical properties has not as yet been investigated. Here we demonstrate that ambient water molecules have a significant influence on the microstructure and performances of ICEs, endowing air-aged ICEs with stable mechanical properties and remarkably boosted conductivity. To decipher the underlying mechanism, we first prepare different types of ICEs and compare their mechanical and electrical performances before and after exposing them to ambient air for a prolonged time (up to 96 hours). In order to rationalize the observed changes in mechanical properties, we carried out atomistic-level simulations by LAMMPS to probe the effect of water molecules on intramolecular interactions between Li^+ , water molecules, and elastomer chains. Finally, we discuss the balance of properties of the ICE in comparison with existing other published studies.

■ MATERIALS AND METHODS

Materials. Lithium bis(trifluoromethane)sulfonimide (LiTFSI), lithium perchlorate (LiClO_4), and Ethylene glycol methyl ether acrylate (MEA) were obtained from Shanghai Aladdin. Isobornyl acrylate (IBA) and benzophenone (BP) were purchased from Shanghai Maklin and Nantong Feiyu, respectively.

Synthesis of the Liquid-Free ICEs. We synthesize two groups of liquid-free ICEs using two representative lithium salts — lithium bis(trifluoromethane)sulfonimide (LiTFSI) and

lithium perchlorate (LiClO_4), respectively, by extending the method introduced previously³⁸. LiTFSI or LiClO_4 is first dissolved in liquid binary mixtures of ethylene glycol methyl ether acrylate (MEA) and isobornyl acrylate (IBA) (shown in Figure 1a). The molar fraction of IBA is fixed to be 0.2 in the binary mixtures and the molar concentration of lithium salts (i.e., LiTFSI and LiClO_4) is taken to be 0.5 M or 1 M in this work. 0.0052 M of benzophenone is added as the photo-initiator. The ICEs are then formed by ultraviolet-induced polymerization for 7.5 h in a nitrogen environment, without any added solvent. The obtained ICEs are named A-x, where A and x represent the name and molar concentration of the lithium salt contained in the ICEs, respectively; For example, LiClO_4 -1 refers to the ICE containing 1 M LiClO_4 . The resulting as-prepared ICEs are lightly crosslinked (due to chain transfer reactions) random copolymer networks of P(MEA-co-IBA) containing mobile cations and anions dispersed throughout the network, and contain no volatile components (Figure 1b). The composition of each sample is given in Table 1 with the molar and weight fraction of monomers and lithium salts.

Table 1. Composition of materials synthesized in this work.

Sample name	Weight fraction of the components (wt%)				Molar fraction of the components			
	MEA	IBA	LiTFSI	LiClO_4	MEA	IBA	LiTFSI	LiClO_4
Copolymer	71.42%	28.57%	0%	0%	80%	20%	0%	0%
LiTFSI -0.5	62.5%	25%	12.5%	0%	74.60%	18.64%	6.76%	0%
LiTFSI -1	55.55%	22.22%	22.23%	0%	69.87%	17.46%	12.67%	0%

LiClO ₄ -0.5	67.79%	27.11%	0%	5.1%	74.54%	18.62%	0%	6.84%
LiClO ₄ -1	64.52%	25.81%	0%	9.67%	69.77%	17.44%	0%	12.79%

Mechanical Characterizations. For all uniaxial-tension tests and cyclic-loading tests, the ICEs were cut into dumbbell-shaped samples, with the sample dimensions specified by the JIS-K6251-7 standard (gauge length: 12 mm, width: 2 mm, and thickness: 2 mm). Pure shear tests were conducted to determine the fracture toughness³⁸, in which two sets of ICE samples are prepared: One set of samples had no pre-crack, while the other set of samples were pre-notched. For all pure-shear samples, the width was 50 mm and the thickness was 2 mm, the distance between the two clamps was 5 mm. The pre-notched sample was prepared by using a razor and had a 25 mm-long single-edge notch. The tests were performed on a universal testing machine (Instron 3343) with a 50 N loading cell. A displacement rate of 100 mm/min was employed for all the tests, yielding a stretch rate of 0.14 s⁻¹ for the uniaxial tension test and 0.33 s⁻¹ for the pure shear tests.

Characterization of Water Uptake. As-prepared liquid-free samples (diameter: 25 mm; thickness: 2 mm) of the ICEs were stored in ambient conditions. Then the weight of the samples was measured at certain intervals (every 3.5 h for the first day, every 12 h for the second day, and every 24 h for the following days). The weight change of each sample was monitored for 4 days (i.e., 96 h).

Molecular Dynamics Simulations. Simulations are carried out using the LAMMPS package and visualization is performed through OVITO software. Recently developed REAX force field⁴⁷ is used to simulate the interactions between lithium salts and polymer chains. We build a simulation box with periodic boundary conditions along the polymerization direction of MEA monomers (Figure S5). There are two polymer chains inside the simulation box, each is polymerized from 8 MEA monomers. The initial size of the simulation box is $1.9 \times 1.8 \times 1.6 \text{ nm}^3$. Then single cation, anion, or water molecule are added to the interface as needed to build corresponding models (e.g., Figure 3a). Such models have the molecular composition close to ICEs used in experiments. The time step in MD is 0.25 fs. In the equilibrium stage, the system is equilibrated at 300 K for 50 ps in the NVT ensemble (Figure S6). In the deformation stage, a carbon atom is fixed on the lower MEA chain skeleton, and the carbon atoms on the upper MEA chain skeleton are displaced along the corresponding direction (Figure S16). For every interval of 0.01 nm in displacement, the energy of the system is minimized, after which the resultant total force of all atoms on the lower MEA chain along the displacement direction is calculated, so that a displacement-force curve is obtained. We change the initial relative position of the molecules (e.g., Li^+ , H_2O) to establish different initial conditions and perform multiple simulations.

Electrical Characterization. A rectangular strip of ICE (dimensions: $40 \times 5 \times 2 \text{ mm}^3$) was prepared using a cutter. The bulk resistance of the samples was measured by a desktop multimeter (Keithley, DAQ 6510). The conductivity of the stretchable ICEs was then calculated

by $\sigma = L/(AR)$, where L corresponds to the distance between the electrodes, A denotes the cross-sectional area of the sample, and R the bulk resistance measured by the multimeter. The conductivity of air-aged samples were measured every 3.5 h for the first day and every 12 h for the following days. The conductivity of each sample was monitored for four days (96 h).

■ RESULTS AND DISCUSSION

Basic properties of the as-prepared ICEs. Figure 1c shows the representative stress-stretch curves of the as-prepared ICEs and pure copolymer P (MEA-co-IBA) (i.e., the polymer backbone of ICEs) before being exposed to ambient air. Due to the low crosslinking level, the as-prepared ICEs exhibit a very large stretch at break with $17 < \lambda_b < 20$. Interestingly, both groups of ICEs possess enhanced stiffness relative to the pure copolymer P (MEA-co-IBA) that contains no lithium salt as well as a pronounced strain hardening at large strain without losing the high stretch at break (Figure 1c, Figure S1 and Figure S2). This stiffening suggests the formation of additional physical bonds between polymer chains and dispersed ions in the ICEs. It is reasonable to hypothesize that strong interactions (namely, lithium bonds) form between Li^+ and carbonyl oxygens on the polymer backbone, and comparatively weaker hydrogen bonds form between anions (TFSI or ClO_4^-) and the chains (as illustrated in Figure 1b)³⁸. Through these intramolecular interactions, Li^+ and associated anions act as transient physical crosslinks among polymer chains, effectively increasing the material's stiffness without decreasing its extensibility. From this molecular picture, ICEs with higher molar concentration of lithium salts should be stiffer, in

agreement with experimental measurements shown in [Figure 1c](#). It is also found that the strength and Young's modulus of LiClO_4 -containing ICEs are roughly three times larger than that of their LiTFSI -containing counterparts with the same salt concentration ([Figure S2](#)), probably because ClO_4^- anions form a different clustering or are better dispersed in comparison with TFSI^- anions.

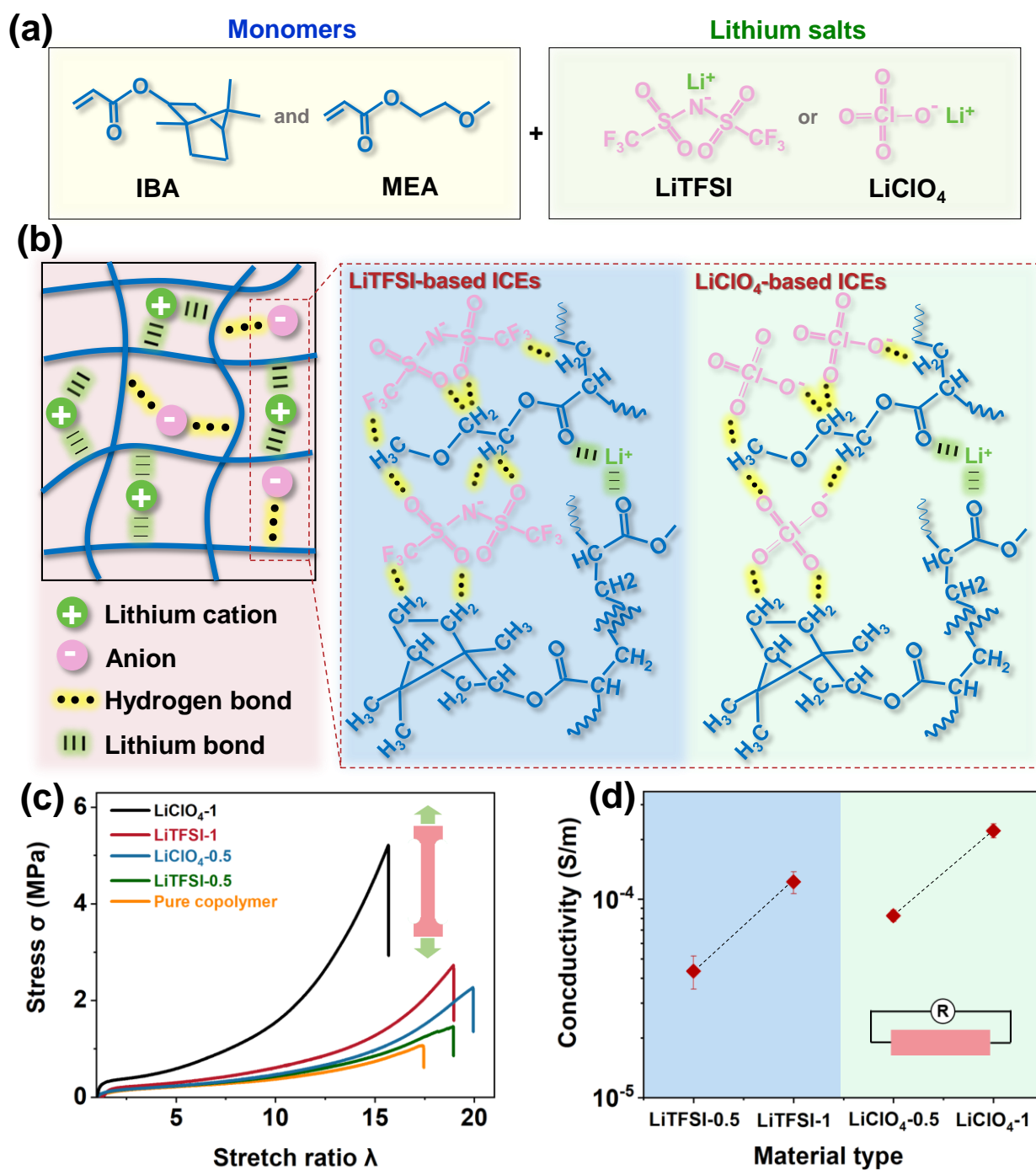


Figure 1. Molecular design and physical properties of the as-prepared liquid-free ICEs. (a) Molecular structures of monomers and lithium salts for the preparation of ICEs. (b) Schematic structure of the ICEs. Two types of ICEs are synthesized by using two distinct lithium salts,

LiTFSI and LiClO₄, respectively. The as-prepared ICEs consist entirely of copolymer network P(MEA-*co*-IBA) and mobile ions and are free of volatile components. Lithium bonds and hydrogen bonds exist between the polymer chains and ions dispersed throughout the network. (c) Representative stress-stretch curves of as-prepared ICEs and the pure copolymer P(MEA-*co*-IBA). The stretch ratio λ is defined as the ratio of the deformed length over the initial length. Note that the ICEs are denoted by A-x, where A= LiTFSI or LiClO₄ and x=0.5 or 1. For example, LiTFSI-0.5 represents the ICE containing 0.5 M LiTFSI. (d) Ionic conductivity of the as-prepared ICEs.

The electrical properties of the as-prepared ICEs are given in [Figure 1d](#). As the salt concentration increases from 0.5 M to 1 M, the ionic conductivity of the as-prepared ICEs increases from 4.35×10^{-5} S/m to 1.22×10^{-4} S/m for LiTFSI-based ICEs, and from 8.26×10^{-5} S/m to 2.23×10^{-4} S/m for LiClO₄-based ICEs. It is noted that the ionic conductivity of the LiClO₄-based ICEs is roughly two times higher than that of their LiTFSI-based counterparts, which pleads for better dispersion of ions in the LiClO₄-based ICEs. Moreover, the ionic conductivity of as-prepared ICEs is lower than that of liquid-based ionic conductors such as ionogels by many orders of magnitude^{12,35,48,49}, mainly because of the lithium and hydrogen bonds formed between polymer chains and ions, which restrict both the motion of polymer chains and transport of ions and thus limit conductivity.

Mechanical properties of air-aged ICEs. To explore the impact of ambient environments on

the mechanical properties of the material, we expose the as-prepared ICEs as well as the pure copolymer P (MEA-*co*-IBA) to ambient air for 96 h and measure their stress-stretch curves every 24 h. As evident from [Figure 2a](#), air-aged ICEs, which are stored in ambient environments for 24 h, soften as compared to their as-made counterparts ([Figure S3](#)). More specifically, [Figure 2b and Figure. 2c](#) show how mechanical properties of the ICEs and copolymers evolve over time under ambient conditions, from which three key observations can be made: (1) The pure copolymer retains its mechanical properties during the entire testing period, indicating that the P (MEA-*co*-IBA) network is insensitive to the ambient environments. (2) By contrast, the air-aged ICEs soften relative to the as-prepared ICEs -- for example, within the first 24 h, Young's modulus and strength of the LiClO₄-1 reduces by a factor of 3.36 and 4.56, respectively -- and, intriguingly, the mechanical properties of all air-aged ICEs are comparable to those of the pure copolymer, regardless of the lithium salt content. (3) After 24 h storage in ambient conditions, the mechanical properties of air-aged ICEs become rather stable, remaining at a comparable level to that of the pure copolymer. As a control experiment, we also age samples of as-made ICEs and copolymer in a dry nitrogen environment (water content \ll 0.01 ppm, oxygen content \ll 0.01 ppm), and found that, for the entire testing period of 96 h, the ICEs stored in the nitrogen environment maintain relatively stable mechanical properties ([Figure S4](#)). Despite the lower modulus and strength, all air-aged ICEs keep the same strain at break similar to ICE samples stored in nitrogen environments ([Figure 2d](#)) as summarized in [Table 2](#).

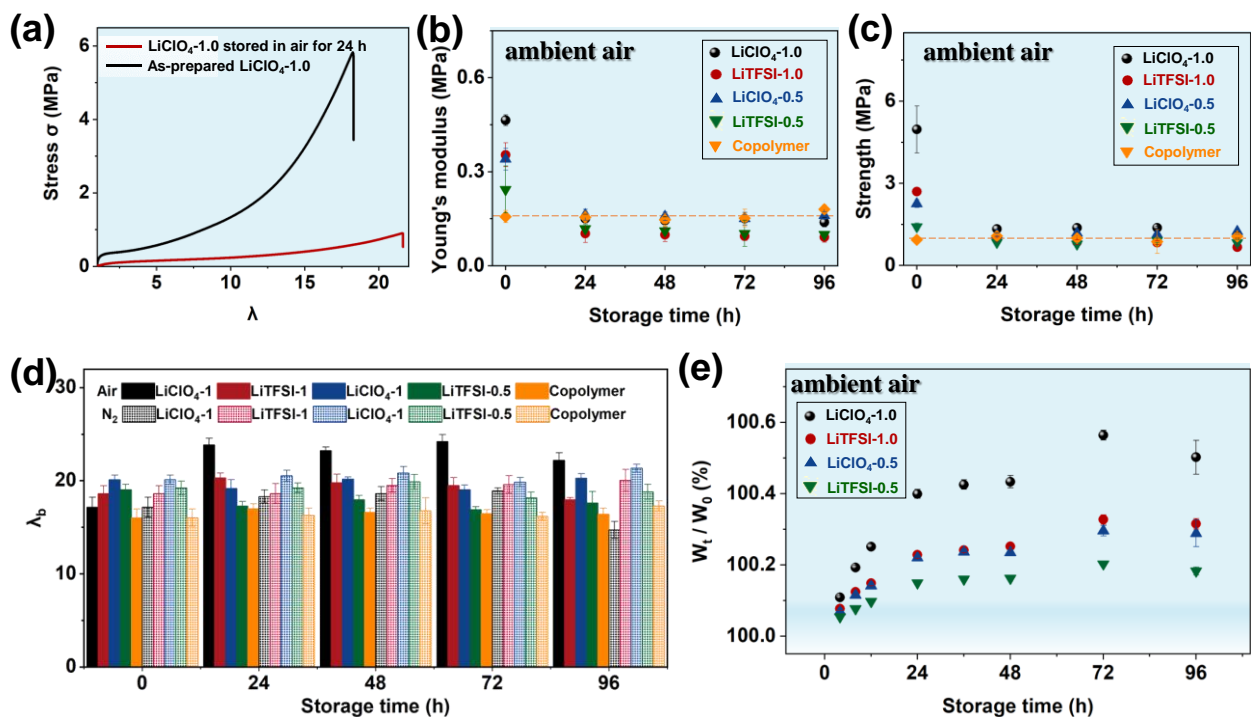


Figure 2. Mechanical properties and weight change of air-aged ICEs. (a) Representative stress-stretch curves of the as-prepared ICE (LiClO₄-1) and that aged in air for 24 h. (b), (c) Young's modulus and tensile strength of the ICEs and the pure copolymer during 96 h storage in ambient air. The values are measured at 24 h intervals. (d) Stretch at break λ_b of ICEs and the pure copolymer stored in air or nitrogen environments. (e) The weight change of the air-aged ICEs due to water absorption when stored in ambient air. Five samples are tested for each data point.

Changes in mechanical properties of the air-aged ICEs could be attributed to the moisture-sensitive nature of the material: The ICEs consist of an elastomer network of P (MEA-*co*-IBA) and mobile ions dispersed throughout the network; although the elastomer network is hydrophobic, the ions are hydrophilic and can absorb environmental water molecules

from ambient air. In this respect, we monitor the weight change of air-aged ICEs over time. After 96 h of storage in ambient air, the ICEs gain a very small amount of weight by absorbing environmental water – approximately 0.35 wt% for LiTFSI-1, 0.2 wt% for LiTFSI-0.5, 0.6 wt% for LiClO₄-1, and 0.35 wt% for LiClO₄-0.5; The higher the content of lithium salt is, the more ambient water is absorbed (Figure 2e). Such a water absorption decreasing the mechanical properties is typically observed in semi-crystalline polymers containing hydrogen bonds or hydrophilic moieties and the best-known example is polyamides⁵⁰. However, it is not commonly observed in elastomers to that extent with such a low amount of water absorption.

Table 2. Summary of mechanical and electrical properties of the air-aged ICEs and the as-prepared ICEs (liquid-free)

	As-prepared				Air-aged (24 h)			
	LiTFSI-0.5	LiClO ₄ -0.5	LiTFSI-1	LiClO ₄ -1	LiTFSI-0.5	LiClO ₄ -0.5	LiTFSI-1	LiClO ₄ -1
Modulus (MPa)	0.24 ±0.07	0.34 ±0.03	0.36 ±0.04	0.47 ±0.02	0.1 ±0.007	0.16 ±0.012	0.09 ±0.016	0.14 ±0.015
Strength (MPa)	1.41 ±0.14	2.25 ±0.14	2.69 ±0.137	4.97 ±0.85	0.83 ±0.106	1.24 ±0.086	0.66 ±0.005	1.09 ±0.112
Stretch at break λ_b	19.02 ±0.61	20.11 ±0.48	18.63 ±0.83	17.15 ±1.06	17.61 ±1.24	20.26 ±0.51	17.97 ±0.22	22.21 ±0.79
Toughness (J m ⁻²)	5862.67 ±282.37	7354.33 ±65.01	8735.33 ±1101.39	26615 ±1901.67	2337.67 ±129.48	3150.67 ±680.52	2961.67 ±746.17	6995 ±687.24
Conductivity (×10 ⁻⁵ S/m)	4.35 ±0.82	8.26 ±0.56	12.22 ±1.54	22.18 ±1.78	63.82 ±7.21	244.44 ±20.90	344.24 ±14.8	1263 ±93.9

Atomistic origins of water-induced modification of air-aged ICEs. Since the high strength and modulus of liquid-free ICEs have been ascribed to dense arrays of physical bonds (namely, lithium bonds and hydrogen bonds) formed between polymer chains and ions³⁸. We hypothesize that the observed changes in mechanical properties observed in air-aged ICEs are a consequence of physical bond scission due to the presence of water molecules. To ascertain our hypothesis and explore the atomistic origins of water-induced modification of the air-aged ICEs, we use molecular dynamics simulations to study the influence of lithium salt as well as water molecules on the interactions between neighboring polymer chains. The lithium salt considered is LiTFSI. We employ a REAX force field recently developed to simulate the effects of lithium salt concentrations in polymer electrolytes⁴⁷. The simulations are carried out in LAMMPS⁵¹. In order to construct models with molecular compositions close to ICEs in experiments, we convert the added amount of monomers and salt during synthesis, and the weight gain due to moisture absorption, into the molar ratio of each constituent component. We estimate that the molar ratio of monomers, LiTFSI, and water is roughly 16:1:1 for LiTFSI-0.5. We only consider the MEA monomers in the simulations because we expect interactions to occur with MEA which is also the majority component. To this end, our simulation is designed to qualitatively probe the inter-chain binding strength between two polymerized MEA chains, modulated by the existence of LiTFSI and water at the interface. To begin with, we build a simulation box with periodic boundary condition along the x-direction (Figure 3a), which is the polymerization direction (i.e., chain direction) of MEA monomers, so that effectively there are two polymer chains aligned in parallel.

Each polymer chain in the simulation box is polymerized from 8 MEA monomers (Figure S5). Then, different interface models (Figure 3a) can be constructed depending on the content that is further added at the interface, while respecting the estimated molar ratio within the simulation box. Since the ICEs are synthesized by dissolving lithium salts in the liquid mixture of monomers, it is expected that the cations and anions are spatially separated along polymer chains after polymerization. For this reason, we consider cations and anions separately in setting up the simulations.

The left panel of Figure 3a shows the Li^+ model in which a single lithium cation is added to the interface, corresponding to the molecular structure of as-prepared ICEs. The system is first equilibrated at 300K in the NVT ensemble in order to form conformed interfaces between the polymer chains and the lithium ion (Figure S6). Then we consider two deformation modes: the interface separation mode (mode 1 in Figure 3a), in which two chains are pulled apart in perpendicular to the backbone direction, and the interface shearing mode (mode 2 in Figure 3a), in which two chains are pulled apart parallel to the backbone direction. The middle panel of Figure 3a shows then the equivalent situation with the $\text{Li}^+/\text{H}_2\text{O}$ model, in which a water molecule is added near the lithium ion. Finally, the right panel of Figure 3a shows the no-addition model, in which neither water molecule nor Li^+ is added. Note that the $\text{Li}^+/\text{H}_2\text{O}$ model and no-addition model represent the microstructure of air-aged ICEs and pure copolymer, respectively. We apply the same simulation procedures for all three models and track the forces on the box along the

pulling directions as a function of displacement.

Figure 3b shows representative displacement-force curves of the three models for mode 1. All curves appear similar in the early stages when the pulling displacement is small (e.g., less than 0.1 nm). However, for the Li^+ model representing as-prepared ICEs, the force evolves to a sharp peak followed by a steep drop, and then decreases gradually to zero. This is in stark contrast with the $\text{Li}^+/\text{H}_2\text{O}$ model (for air-aged ICEs) and the no-addition model (for pure copolymer), where the sharp peaks are not observed and the resultant forces remain relatively low (Figure 3b). To understand the atomistic origin of the sharp peak force in Li^+ model, we examine carefully the change in the molecular configuration of the interface before and after the occurrence of the sharp peak force (insets 1 and 2 of Figure 3b). We find that initially the lithium ion bonds simultaneously to both polymer chains via the carbonyl oxygens, forming two chain-connecting lithium bonds (two purple arrows in inset 1 of Figure 3b), which are maximally stretched as the force reaches the peak, until one chain-connecting lithium bond fractures (inset 2 of Figure 3b), giving rise to the sharp drop of the force. In contrast, in the $\text{Li}^+/\text{H}_2\text{O}$ model, after the equilibration stage, we find that the water molecule bonds to the lithium ion (dashed lines in insets 1' - 3' in Figure 3b), leaving only one chain-connecting lithium bond (arrow in insets 1' - 3' in Figure 3b). In other words, in the presence of a nearby water molecule, the lithium ion is not able to simultaneously interact with both polymer chains. As a result, during chain separation, no lithium bonds are fractured and the resulting force is much smoother and lower than that of the

Li^+ model (Figure 3b). Therefore, the formation of lithium ions that simultaneously bind to both polymer chains via chain-connecting lithium bonds is the key mechanism strengthening the interface as well as the entire as-prepared ICE. Due to the lack of such mechanism both in $\text{Li}^+/\text{H}_2\text{O}$ model and in the no-addition model, the corresponding forces resisting deformation are much lower and broadly similar. This result is consistent with the experimental observation in Figure 2b and 2c that as-prepared ICEs exhibit higher modulus and strength than air-aged ICEs and pure copolymer, and that the air-aged ICEs and pure copolymer have similar modulus and strength. We have done 10 groups of simulations with different initial conditions and all results support the above observation (Figure S7).

Figure 3c shows representative displacement-force curves of the three models for mode 2. Two sharp peaks of force appear in the Li^+ model. The sharp peaks indicate the repeated scission and reforming of the chain-connecting lithium bonds, and can be seen from molecular configurations of the interface (insets 1-3 of Figure 3c). Initially the lithium ion bonds to both polymer chains, forming two chain-connecting lithium bonds (two purple arrows in inset 1 of Figure 3c), which are stretched to their critical state (the first peak) during polymer chain sliding, until one of the chain-connecting lithium bonds breaks (inset 2 of Figure 3c). As the sliding continues, when the lithium ion captures a new chain-connecting site, then a new chain-connecting lithium bond reforms (Figure 3c, inset 3), restoring a lithium ion that simultaneously links both polymer chains. The above scission and reforming processes repeats

during the sliding process, giving rise to another sharp force peak (Figure 3c). A cascade of such lithium bond scission and reforming events can dissipate a significant amount of energy, and thus result in high fracture toughness of as-prepared ICEs³⁸. In contrast, for the Li⁺/H₂O model, the lithium ion cannot simultaneously form lithium bonds with two polymer chains in the presence of nearby water molecule. Therefore, no lithium bonds are fractured during chain sliding (insets 1' and 2' of Figure 3c), thereby giving rise to much smoother and lower resultant force. Likewise, due to the lack of energy dissipation mechanism (i.e., the scission and reforming of chain-connecting lithium bonds) in no-addition model, the resistant force is similar to that of the Li⁺/H₂O model. 10 groups of simulations for mode 2 with different initial conditions have been carried out and all results agree well with the above observation (Figure S8).

For the case of TFSI⁻ anions, the simulation results (Figures S9-S11) indicate that the weakening effect induced by the water molecule does not appear for the interface shearing mode (Figure S11), but remains present for the interface separation mode (Figure S10). In summary, results from molecular dynamics simulations strongly suggest that the molecular mechanism of water-induced modifications of the air-aged ICEs is mainly the scission of chain-connecting lithium bonds induced by water absorption. The dynamic lithium bonds between Li⁺ and carbonyl oxygens on the polymer backbone prefer to dissociate when water molecules come nearby. Hence, the diffusing water molecules in the air-aged ICEs accelerate the exchange rate of the lithium bonds to a level far beyond the loading rate, thereby rendering the lithium bonds

mechanically invisible and effectively diminishing the number of lithium bonds^{52,53}, eventually giving rise to the water-induced modifications of the air-aged ICEs.

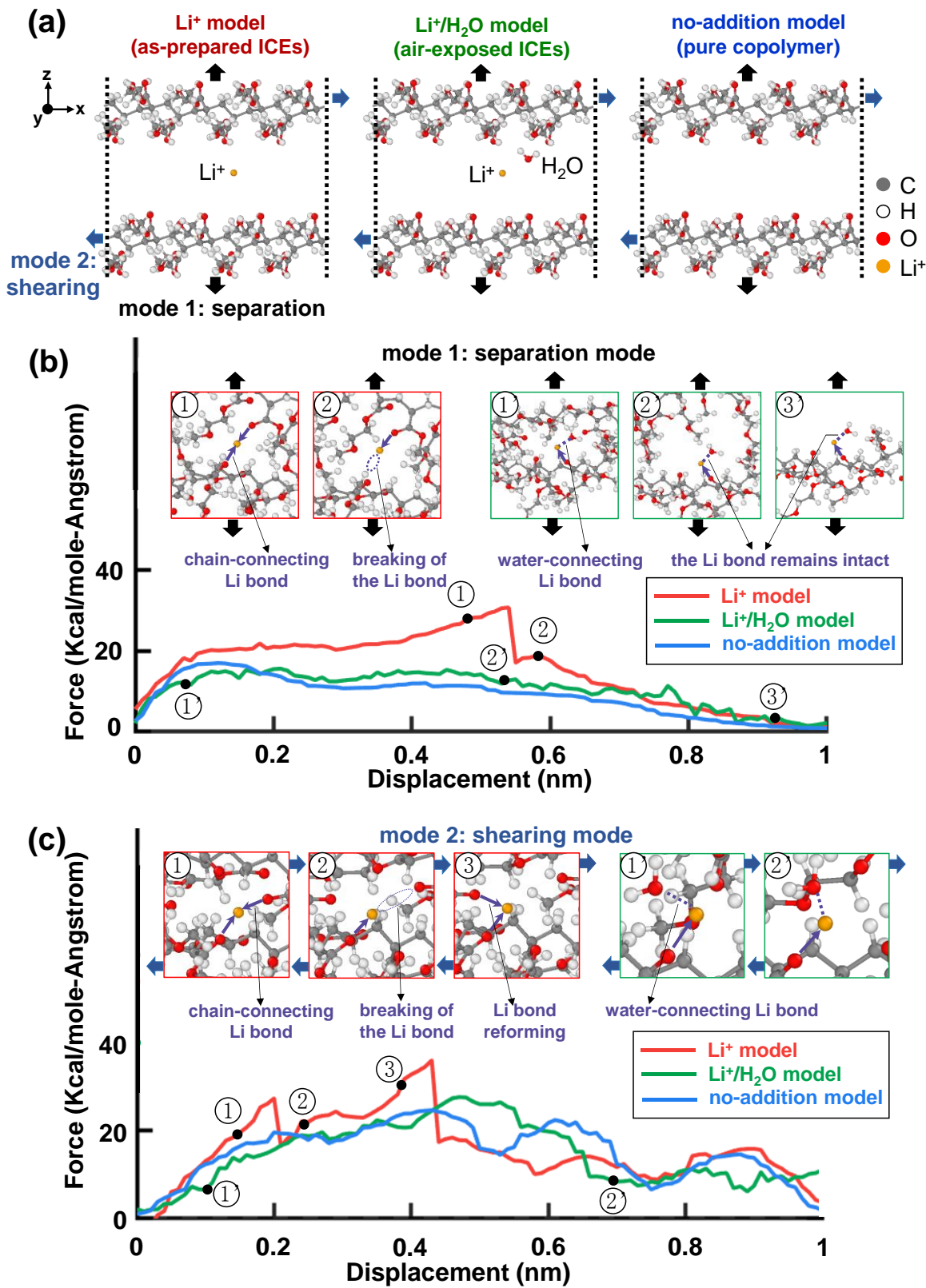


Figure 3. Atomistic origins of water-induced modification of air-aged ICEs. (a) Pre-equilibration

molecular models corresponding to the molecular structures of as-prepared ICEs, air-aged ICEs, and pure copolymers, respectively. Left to right: Li^+ model (i.e., as-prepared ICEs), $\text{Li}^+/\text{H}_2\text{O}$ model (air-aged ICEs), no-addition model (pure copolymer). The dashed lines denote periodic boundaries so that there are effectively two chains polymerized from MEA monomers. The arrows represent loading directions for the two deformation modes imposed after equilibration. Mode 1 represents chain separation and mode 2 represents chain sliding. (b) Representative force-displacement curves of mode 1. The insets show the molecular configurations of the interface at the points labeled on the curves. The purple arrows represent the chain-connecting lithium bonds and the dashed lines represent water-connecting lithium bonds. Insets 1 to 2 show the fracture of a chain-connecting lithium bond. Insets 1' to 3' show that the single chain-connecting lithium bond in $\text{Li}^+/\text{H}_2\text{O}$ model is stable. (c) Representative force-displacement curves of mode 2. The insets 1 to 3 show the breaking and reformation processes of a pair of chain-connecting lithium bonds in the Li^+ model. The insets 1' to 2' show that the single chain-connecting lithium bond in the $\text{Li}^+/\text{H}_2\text{O}$ model remains stable, so that the energy dissipation mechanism due to bond breaking and reforming is absent.

Fracture resistance and elastic recovery of air-aged ICEs. Though affected by water molecules in ambient air, air-aged ICEs exhibit excellent fracture resistance and a highly elastic behavior with rapid recovery, an important property for practical applications of ICEs in ambient environments. We measure the fracture toughness Γ of both as-prepared and air-aged ICEs using

the pure-shear geometry⁵⁴, as well as the work of fracture W of the ICEs by the uniaxial tension test. Although the fracture toughness and work of fracture of the air-aged ICEs are smaller than that of as-made ICEs (Figure 4a and 4b), the air-aged ICEs still possess high fracture toughness. For example, after absorbing environmental water molecules, the ICE LiClO₄-1 exhibit a fracture toughness of ~ 7000 J/m² and work of fracture of ~ 10 MJ/m³ (Figure 4a), exceeding that of most other state-of-the-art soft ionic conductors^{12,13,48,55-57}. We also evaluate the fractocohesive length of both as-prepared and air-aged ICEs, which is defined as the ratio of fracture toughness over work of fracture (i.e., Γ/W)^{58,59}. The fractocohesive length characterizes the flaw sensitivity of materials: the stretchability of material is insensitive to any flaw of the size smaller than its fractocohesive length. LiTFSI-based ICEs present a fractocohesive length of ~ 0.46 - 0.48 mm, while the LiClO₄-based ICEs have a fractocohesive length of ~ 0.4 - 0.7 mm and these values are comparable to those of the liquid-free as-prepared ICEs (Figure 4c).

To explore the elastic recovery of ICEs, we subject as-prepared and air-aged ICEs of all types to a cycle of loading and unloading with the maximum stretch of $\lambda_{max} = 11$ and a strain rate of 0.14 s⁻¹. The hysteresis of an ICE sample is represented by the dissipated energy U_d , the area between the loading and unloading stress-stretch curves. Unlike as-prepared ICE samples, which exhibit hysteresis loops depending on both the type and concentration of lithium salt³⁸, the air-aged ICEs exhibit almost identical hysteresis loops, regardless of the salt type and concentration (Figure 4d, Figure S12). This observation is consistent with the molecular

dynamics simulation: As-prepared ICEs contain a large number of chain-connecting lithium bonds and hydrogen bonds connecting polymer chains – the amount of which largely depends on the salt type and concentration – and the repeated breaking and reforming of these physical bonds dissipate energy^{60,61}. In contrast, relative to their as-prepared counterparts, air-aged ICEs effectively contain much fewer, if any, load-bearing lithium bonds linking adjacent chains due to the competition with water molecules. This difference also results in a lower residual stretches for air-aged ICEs at a given strain rate (Figure S13). The enhanced elastic recovery ratio may arise from the plasticizing effect of water molecules, which facilitate chain motion by effectively reducing chain-connecting lithium bonds, as informed by the molecular dynamics simulations. To further investigate the elastic recovery behavior of air-aged ICEs under cyclic loadings, we cyclically stretch air-aged LiTFSI-0.5 to increasing maximum stretch levels ($\lambda_{max}=3$ to $\lambda_{max}=15$). The ICE is highly elastic with fast self-recovery, having an ultimate recovery ratio of 93.2% and a corresponding residual stretch of only $\lambda_{res} = 1.95$ as released from $\lambda_{max} = 15$ (Figure 4e, Figure S14). The dissipated energy associated with each cycle increases almost linearly with λ_{max} (Figure 4f). The air-aged LiTFSI-0.5 also demonstrates low hysteresis and small residual strains when subjected to 100 successive loading-unloading cycles with $\lambda_{max} = 6$ and $\lambda_{max} = 11$ (Figure S15). These results indicate a highly elastic behavior of air-aged ICEs with rapid recovery and low hysteresis, a trait highly desirable for soft ionotronic devices.

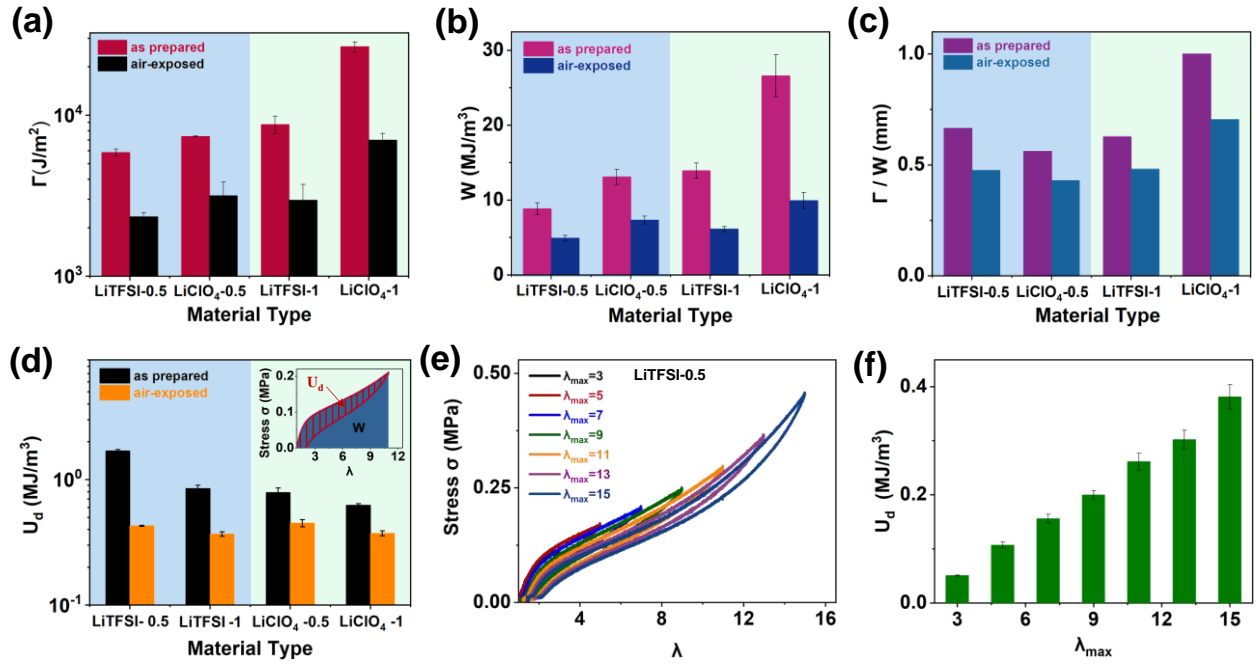


Figure 4. Fracture resistance, hysteresis, and elastic recovery of air-aged ICEs. (a) Fracture toughness Γ of ICEs. (b) Work of fracture W of ICEs. (c) Fractocohesive length Γ/W of the ICEs. (d) Dissipated energy U_d of air-aged ICEs for $\lambda_{max} = 11$. The inset is the loading-unloading curve of an air-aged LiClO₄-0.5 sample stretched to $\lambda_{max} = 11$. The dissipated energy U_d is represented by the area between the loading-unloading curves. (e) Step-strain loading-unloading curves of air-aged LiTFSI-0.5 sample cyclically stretched to different λ_{max} . (f) Corresponding strain-dependent dissipated energy for LiTFSI-0.5. In this figure, air-aged ICEs refer to ICE samples stored in air for 24 h before testing. Three samples are tested for each data point.

Enhanced ionic conductivity of the air-aged ICEs. As discussed above, after 96 h storage under ambient conditions, the air-aged ICEs can absorb from the humid air a low amount of

ambient water – no more than ~0.6 wt% for all types of ICEs tested in this work (Figure 2e), with the molar concentration of absorbed water molecules being comparable to that of Li cations in the ICEs. Notably, such a limited amount of ambient water uptake can boost the ionic conductivity of the air-aged ICEs by one to two orders of magnitude. For example, LiClO₄-1 possesses an ionic conductivity of $1.26 \times 10^{-2} \text{ S/m}$ after 96 h exposure to ambient air, which is ~57 times larger than its conductivity measured in the as-prepared liquid-free state (Figure 5a, Table 2). The basic mechanism underpinning the enhanced conductivity can be understood as follows: In as-prepared ICEs, as revealed by the molecular dynamics simulation results, Li⁺ acts as transient physical crosslinks to connect neighboring polymer chains via chain-connecting lithium bonds, restricting the motion of both the polymer chains and the ions. By contrast, in the presence of water molecules, Li⁺ must exchange much faster with the carboxyl bonds due to the competition with water and effectively become much more mobile, thus leading to a significantly increased conductivity. The air-aged ICEs reported in this work exhibit a conductivity comparable to that of recently-reported ionogels^{12,35,48}, yet containing much less liquid content than ionogels do, thereby reducing the hassles of leaking liquid materials to a minimum. The conductivity of the air-aged ICEs and as-prepared ICEs are listed in Table 2 for reference.

Comparison of air-aged ICEs to other state-of-the-art soft ionic conductors. The development of ICEs started around 2018, and since then ICEs have been incorporated in many applications, including ionic skins, triboelectric nanogenerators, and touch screens^{36,38,43,46,62},

owing to their liquid-free nature as well as ideal combination of mechanical and electrical characteristics. In this work, it is found that although the exposure to ambient water causes a reduction in modulus and strength of the ICEs, the stretchability remains the same, elastic recovery is slightly increased and the ionic conductivity is remarkably improved. In other words, the air-aged ICEs still present a desirable combination of stable mechanical properties and enhanced conductivity. To show this, we compare air-aged ICEs (namely, $\text{LiClO}_4\text{-1}$) to other state-of-the-art ionic conductors, including liquid-free ICEs, ionoelastomers, and ionogels, in terms of Young's modulus, strength, stretchability, and conductivity. We found that the air-aged ICEs are a highly competitive candidate material for soft ionotronics since they possess an overall performance similar to the most advanced stretchable ionic conductors reported very recently (Figure 5b, Table S1). Thanks to the very limited amount of water absorbed from ambient air, the air-aged ICEs outperform most liquid-free ICEs and ionoelastomers in terms of conductivity and are superior to liquid-based ionic conductors (e.g., hydrogels and ionogels) for long-term applications as the latter inevitably suffer from liquid leakage and evaporation.

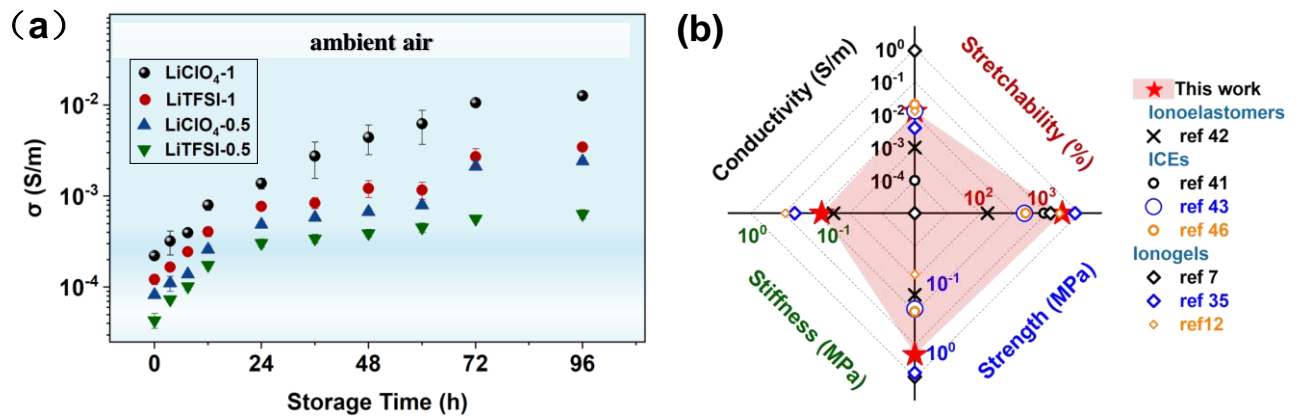


Figure 5. Comparison of air-aged ICEs to other state-of-the-art soft ionic conductors. (a) The conductivity increases of air-aged ICEs during 96 h storage under ambient conditions. 3-4 samples are tested for each data point. (b) Radar chart that compares representative air-aged ICEs (LiClO₄-1) to recently-reported soft ionic conductors in terms of modulus, strength, stretchability, and conductivity.

■ CONCLUSIONS

In this work, we report a first-of-its-kind study of the impact of ambient water on mechanical and electrical performances of ICEs. We identify that the hygroscopic nature of lithium ions causes the ICEs to absorb a very low amount of water, approximately one water molecule per lithium ion, resulting in a ~0.3-0.6 wt% weight gain. Experimental measurements together with molecular dynamics simulations reveal that these water molecules – though in very limited amount -- can cause scission of lithium bonds between lithium ions and polymer chains on the molecular scale and speed up the bond exchange rate^{53,63}, giving rise to a number of changes in mechanical and electrical properties of the ICEs at the macroscopic scale. First, Li ions in as-prepared ICEs act as relatively slow exchanging physical crosslinks by connecting adjacent polymer chains via lithium bonds, the accelerated exchanging of these chain-connecting lithium bonds effectively diminishes the number of visible ‘physical crosslinks’, leading to reduced but stable modulus and strength of the air-aged ICEs. Second, the large number of lithium bonds in as-prepared ICEs may break and reform during deformation, dissipating a

significant amount of energy and leading to pronounced hysteresis. The air-aged ICEs effectively contain much fewer visible chain-connecting lithium bonds due to the accelerated bond exchange induced by diffusing water molecules, thereby exhibiting lower hysteresis and improved self-recovery. Third, the water-absorption-induced breakage and accelerated exchange of chain-connecting lithium bonds facilitate the motion of polymer chains and the transport of ions, which results in increased stretchability and significantly enhanced conductivity. In summary, air-aged ICEs possess competent mechanical and electrical properties that are comparable to other state-of-the-art soft ionic conductors and, more importantly, can outperform liquid-free (e.g., ionoelastomers, as-made ICEs) and liquid-based (e.g., ionogels) soft ionic conductors in terms of conductivity and stability, respectively, by taking advantage of the small amount of ambient water contained. We anticipate our result will shed light on the practical mass applications of ICE-based ionotronic devices in ambient air.

■ ASSOCIATED CONTENT

Supporting Information

Additional information and figures.

■ AUTHOR INFORMATION

Corresponding Author

*E-mail: (C. Creton) costantino.creton@espci.psl.eu; (Z. Jia) zheng.jia@zju.edu.cn; (S.Z. Zhu)

shuzezhu@zju.edu.cn

Author Contribution

[§]B.R.B. Yiming and Z.X. Zhang contributed equally. B.R.B. Yiming designed the study, synthesized the samples, conducted the experiments, processed and analyzed the data, and co-wrote the manuscript. Z.X. Zhang and Prof. S.Z. Zhu carried out the molecular dynamics simulations and co-wrote the manuscript. Y.C. Lu measured the weight and ionic conductivity of the samples. Prof. X.G. Liu helped with the design of LiClO₄-based ICEs. Prof. Z. Jia conceived the idea, Prof. Z. Jia and Prof. C. Creton supervised the project, co-wrote and revised the manuscript, Prof. S.X. Qu discussed the results and revised the manuscript.

Notes

The authors declare no competing financial interest.

■ ACKNOWLEDGMENTS

This work is supported by the National Natural Science Foundation of China (Grant Nos. 11802269, 12072314, and 12002304), the 111 Project (Grant No. B21034), and the One-Hundred Talents Program of Zhejiang University.

■ REFERENCES

- 1 Canhui Yang, Z. S. Hydrogel iontronics. *Nat. Rev. Mater.* **3**, 125-142 (2018).
- 2 Yang Can Hui , C. B., Lu Jing Jing, Yang Jian Hai, Zhou Jinxiong, Chen Yong Mei, Suo Zhigang. Ionic cable. *Extreme. Mech. Lett.* **3**, 59-65 (2015).
- 3 Tiefeng Li, G. L., Yiming Liang, Tingyu Cheng, Jing Dai, Xuxu Yang, Bangyuan Liu, Zedong Zeng, Zhilong Huang, Yingwu Luo, Tao Xie, Wei Yang. Fast-moving soft electronic fish. *Sci. Robot.* **3**, e1602045 (2017).
- 4 Younghoon Lee *et al.* Ionic spiderwebs. *Sci. Robot.* **5** (2020).
- 5 Chong-Chan Kim, H.-H. L., Kyu Hwan Oh, Jeong-Yun Sun. Highly stretchable, transparent ionic touch panel. *Science* **353**, 682-687 (2021).
- 6 Xiong Pu, M. L., Xiangyu Chen, Jiangman Sun, Chunhua Du, Yang Zhang, Junyi Zhai, Weiguo Hu, Zhong Lin Wang. Ultrastretchable, transparent triboelectric nanogenerator as electronic skin for biomechanical energy harvesting and tactile sensing. *Sci. Adv.* **3**, e1700015 (2017).
- 7 Yongyuan Ren, J. G., Ziyang Liu, Zhe Sun, Yiqing Wu, Lili Liu, Feng Yan. Ionic liquid-based click-ionogels. *Sci. Adv.* **5**, eaax0648 (2019).
- 8 Zhang, P. *et al.* Stretchable, Transparent, and Thermally Stable Triboelectric Nanogenerators Based on Solvent-Free Ion-Conducting Elastomer Electrodes. *Adv. Funct. Mater.* **30**, 1909252 (2020).

- 9 Guoying Gu, H. X., Sai Peng, Ling Li, Sujie Chen, Tongqing Lu, and Xiaojun Guo. Integrated Soft Ionotronic Skin with Stretchable and Transparent Hydrogel-Elastomer Ionic Sensors for Hand-Motion Monitoring. *Soft robotics* **6**, 368-376, doi:10.1089/soro.2018.0116 (2019).
- 10 Binbin Ying, Qiyang Wu, Jianyu Li & Liu, a. X. An ambient-stable and stretchable ionic skin with multimodal sensation. *Mater. Horiz.* **7**, 477-488, doi:10.1039/c9mh00715f (2020).
- 11 Qiao Wang *et al.* A dual-trigger-mode ionic hydrogel sensor for contact or contactless motion recognition. *Mater. Horiz.* **7**, 2673-2682 (2020).
- 12 Yiming, B. *et al.* Ambiently and Mechanically Stable Ionogels for Soft Ionotronics. *Advanced Functional Materials*, doi:10.1002/adfm.202102773 (2021).
- 13 Yang, C. H., Zhou, S., Shian, S., Clarke, D. R. & Suo, Z. Organic liquid-crystal devices based on ionic conductors. *Materials horizons* **4**, 1102-1109, doi:10.1039/c7mh00345e (2017).
- 14 Lim, S. M. *et al.* Ion-to-ion amplification through an open-junction ionic diode. *Proceedings of the National Academy of Sciences of the United States of America* **116**, 13807-13815, doi:10.1073/pnas.1903900116 (2019).
- 15 Han, Z. *et al.* Dual pH-Responsive Hydrogel Actuator for Lipophilic Drug Delivery. *ACS applied materials & interfaces* **12**, 12010-12017, doi:10.1021/acsami.9b21713 (2020).
- 16 Liu, B. *et al.* Hydrogel Coating Enabling Mechanically Friendly, Step - Index, Functionalized Optical Fiber. *Advanced Optical Materials*, doi:10.1002/adom.202101036 (2021).
- 17 Liu, J., Qu, S., Suo, Z. & Yang, W. Functional hydrogel coatings. *National Science Review* **8**, doi:10.1093/nsr/nwaa254 (2021).

- 18 Sun, J. Y., Keplinger, C., Whitesides, G. M. & Suo, Z. Ionic skin. *Adv Mater* **26**, 7608-7614, doi:10.1002/adma.201403441 (2014).
- 19 Lei, Z., Wang, Q., Sun, S., Zhu, W. & Wu, P. A Bioinspired Mineral Hydrogel as a Self-Healable, Mechanically Adaptable Ionic Skin for Highly Sensitive Pressure Sensing. *Adv. Mater.* **29**, doi:10.1002/adma.201700321 (2017).
- 20 Wang, Y. *et al.* Extremely stretchable and healable ionic conductive hydrogels fabricated by surface competitive coordination for human-motion detection. *Chemical Engineering Journal* **420**, doi:10.1016/j.cej.2020.127637 (2021).
- 21 C. Larson, B. P., S. Li, S. Robinson, M. Totaro, L. Beccai, B. Mazzolai, R. Shepherd. Highly stretchable electroluminescent skin for optical signaling and tactile sensing. *Science*, 1071-1073 (2016).
- 22 Yang, C. H., Chen, B., Zhou, J., Chen, Y. M. & Suo, Z. Electroluminescence of Giant Stretchability. *Adv Mater* **28**, 4480-4484, doi:10.1002/adma.201504031 (2016).
- 23 Yang, C. *et al.* Ionotronic Luminescent Fibers, Fabrics, and Other Configurations. *Adv Mater* **32**, e2005545, doi:10.1002/adma.202005545 (2020).
- 24 Bai, Y. *et al.* Transparent hydrogel with enhanced water retention capacity by introducing highly hydratable salt. *Applied Physics Letters* **105**, doi:10.1063/1.4898189 (2014).
- 25 Yuk, H., Lu, B. & Zhao, X. Hydrogel bioelectronics. *Chemical Society reviews*, doi:10.1039/c8cs00595h (2018).
- 26 Liu, X., Liu, J., Lin, S. & Zhao, X. Hydrogel machines. *Materials Today* **36**, 102-124,

doi:10.1016/j.mattod.2019.12.026 (2020).

27 Hyunwoo Yuk, T. Z., Shaoting Lin, German Alberto Parada, and Xuanhe Zhao. Tough bonding of hydrogels to diverse non-porous surfaces. *Nat Mater* **15**, 190-198, doi:10.1038/nmat4463 (2016).

28 Takayuki Nonoyama, S. W., Ryuji Kiyama, Nobuto Kitamura, Md. Tariful Islam Mredha, Xi Zhang, Takayuki Kurokawa, Tasuku Nakajima, Yasuaki Takagi, Kazunori Yasuda, and Jian Ping Gong. Double-Network Hydrogels Strongly Bondable to Bones by Spontaneous Osteogenesis Penetration. *advmat*, doi:10.1002/adma.201601030 (2016).

29 Qihan Liu, G. N., Canhui Yang, Shaoxing Qu, and Zhigang Suo. Bonding dissimilar polymer networks in various manufacturing processes. *Nature communications* **9**, 846, doi:10.1038/s41467-018-03269-x (2018).

30 Gao, Y. *et al.* A Universal Strategy for Tough Adhesion of Wet Soft Material. *Advanced Functional Materials* **30**, doi:10.1002/adfm.202003207 (2020).

31 Qi Ge, Z. C., Jianxiang Cheng, Biao Zhang, Yuan-Fang Zhang, Honggeng Li, & Xiangnan He, C. Y., Ji Liu, Shlomo Magdassi, Shaoxing Qu. 3D printing of highly stretchable hydrogel with diverse UV curable polymers. *science advances* **7**, eaba4261 (2021).

32 Le Bideau, J., Viau, L. & Vioux, A. Ionogels, ionic liquid based hybrid materials. *Chemical Society reviews* **40**, 907-925, doi:10.1039/c0cs00059k (2011).

33 Wang, H. *et al.* Ionic Gels and Their Applications in Stretchable Electronics. *Macromolecular rapid communications*, e1800246, doi:10.1002/marc.201800246 (2018).

34 Correia, D. M. *et al.* Ionic Liquid–Polymer Composites: A New Platform for Multifunctional Applications. *Advanced Functional Materials* **30**, doi:10.1002/adfm.201909736 (2020).

35 Cao, Z., Liu, H. & Jiang, L. Transparent, mechanically robust, and ultrastable ionogels enabled by hydrogen bonding between elastomers and ionic liquids. *Materials Horizons* **7**, 912-918, doi:10.1039/c9mh01699f (2020).

36 Lei, Z. W., P. A highly transparent and ultra-stretchable conductor with stable conductivity during large deformation. *Nat. Commun.* **10**, 3429 (2019).

37 Chen, B. *et al.* Highly stretchable and transparent ionogels as nonvolatile conductors for dielectric elastomer transducers. *ACS. Appl. Mater. Interfaces.* **6**, 7840-7845, doi:10.1021/am501130t (2014).

38 Yiming, B. *et al.* A Mechanically Robust and Versatile Liquid-Free Ionic Conductive Elastomer. *Adv Mater* **33**, e2006111, .

39 Kim, Y. M. & Moon, H. C. Ionoskins: Nonvolatile, Highly Transparent, Ultrastretchable Ionic Sensory Platforms for Wearable Electronics. *Advanced Functional Materials* **30**, doi:10.1002/adfm.201907290 (2019).

40 Seo, D. G. & Moon, H. C. Mechanically Robust, Highly Ionic Conductive Gels Based on Random Copolymers for Bending Durable Electrochemical Devices. *Advanced Functional Materials* **28**, doi:10.1002/adfm.201706948 (2018).

41 Shi, L. *et al.* Highly stretchable and transparent ionic conducting elastomers. *Nature*

communications **9**, 2630, doi:10.1038/s41467-018-05165-w (2018).

42 Hyeong Jun Kim, B. C., Zhigang Suo, Ryan C. Hayward. Ionoelastomer junctions between polymer networks of fixed anions and cations. *Science* **367**, 773–776 (2020).

43 Qu, X. *et al.* Solid-state and liquid-free elastomeric ionic conductors with autonomous self-healing ability. *Materials horizons* **7**, 2994–3004, doi:10.1039/d0mh01230k (2020).

44 Dang, C. *et al.* Facile solvent-free synthesis of multifunctional and recyclable ionic conductive elastomers from small biomass molecules for green wearable electronics. *Journal of Materials Chemistry A* **9**, 13115–13124, doi:10.1039/d1ta01659h (2021).

45 Wang, M. *et al.* Multifunctional Liquid-Free Ionic Conductive Elastomer Fabricated by Liquid Metal Induced Polymerization. *Advanced Functional Materials*, doi:10.1002/adfm.202101957 (2021).

46 Zhang, P. *et al.* Dynamically Crosslinked Dry Ion-Conducting Elastomers for Soft Iontronics. *Adv Mater*, e2101396, doi:10.1002/adma.202101396 (2021).

47 Liu, Y. *et al.* Effects of High and Low Salt Concentrations in Electrolytes at Lithium-Metal Anode Surfaces Using DFT-ReaxFF Hybrid Molecular Dynamics Method. *J Phys Chem Lett* **12**, 2922–2929, doi:10.1021/acs.jpcclett.1c00279 (2021).

48 Lei Shi, K. J., Yiyang Gao, Hua Yang, Yaming Ma, Shiyao Lu, Guoxin Gao, Huaitian Bu, Tongqing Lu, and Shujiang Ding Highly Stretchable and Transparent Ionic Conductor with Novel Hydrophobicity and Extreme-Temperature Tolerance. *Research* **2020**, 1–10, doi:10.34133/2020/2505619 (2020).

- 49 Cho, K. G. *et al.* Block Copolymer-Based Supramolecular Ionogels for Accurate On-Skin Motion Monitoring. *Advanced Functional Materials*, doi:10.1002/adfm.202102386 (2021).
- 50 Silva, L., Tognana, S. & Salgueiro, W. Study of the water absorption and its influence on the Young's modulus in a commercial polyamide. *Polymer Testing* **32**, 158-164, doi:10.1016/j.polymertesting.2012.10.003 (2013).
- 51 Plimpton, S. Fast Parallel Algorithms for Short-Range Molecular Dynamics. *J Comp Phys* **117**, 1-19 (1995).
- 52 Mayumi, K., Guo, J., Narita, T., Hui, C. Y. & Creton, C. Fracture of dual crosslink gels with permanent and transient crosslinks. *Extreme Mechanics Letters* **6**, 52-59, doi:10.1016/j.eml.2015.12.002 (2016).
- 53 Kean, Z. S. *et al.* Increasing the maximum achievable strain of a covalent polymer gel through the addition of mechanically invisible cross-links. *Adv Mater* **26**, 6013-6018, doi:10.1002/adma.201401570 (2014).
- 54 Jeong-Yun Sun, X. Z., Widusha R. K. Illeperuma, Ovijit Chaudhuri, Kyu Hwan Oh, David J. Mooney, Joost J. Vlassak, Zhigang Suo. Highly stretchable and tough hydrogels.pdf. *nature* (2012).
- 55 Sun, T. L. *et al.* Physical hydrogels composed of polyampholytes demonstrate high toughness and viscoelasticity. *Nat Mater* **12**, 932-937, doi:10.1038/nmat3713 (2013).
- 56 Feng Luo , T. L. S., Tasuku Nakajima , Takayuki Kurokawa , Yu Zhao , Koshiro Sato , & Abu Bin Ihsan , X. L., Honglei Guo , and Jian Ping Gong. Oppositely Charged Polyelectrolytes

Form Tough,

Self-Healing, and Rebuildable Hydrogels. *advmat*, doi:10.1002/adma.201500140 (2015).

57 Hong, S. *et al.* 3D Printing of Highly Stretchable and Tough Hydrogels into Complex, Cellularized Structures. *Adv Mater* **27**, 4035-4040, doi:10.1002/adma.201501099 (2015).

58 Chao Chen, Zhengjin Wang & Suo., Z. Flaw sensitivity of highly stretchable materials. *Extreme. Mech. Lett.* **10**, 50-57, doi:10.1016/j.eml.2016.10.002 (2017).

59 Canhui Yang, Tenghao Yin & Suo, Z. Polyacrylamide hydrogels. I. Network imperfection. *J. Mech. Phys. Solids.* **131**, 43-55, doi:10.1016/j.jmps.2019.06.018 (2019).

60 Long, R., Mayumi, K., Creton, C., Narita, T. & Hui, C.-Y. Time Dependent Behavior of a Dual Cross-Link Self-Healing Gel: Theory and Experiments. *Macromolecules* **47**, 7243-7250, doi:10.1021/ma501290h (2014).

61 Guo, J., Long, R., Mayumi, K. & Hui, C.-Y. Mechanics of a Dual Cross-Link Gel with Dynamic Bonds: Steady State Kinetics and Large Deformation Effects. *Macromolecules* **49**, 3497-3507, doi:10.1021/acs.macromol.6b00421 (2016).

62 Zhang, P. *et al.* Stretchable, Transparent, and Thermally Stable Triboelectric Nanogenerators Based on Solvent-Free Ion-Conducting Elastomer Electrodes. *Advanced Functional Materials* **30**, doi:10.1002/adfm.201909252 (2020).

63 Costantino Creton, Oguz O. Self-Healing and Self-Recovering Hydrogels. *Advances in Polymer Science* **285**, V-VI (2020).

